SCIENCE CHINA
Information Sciences

• LETTER •

September 2026, Vol. 69, Iss. 9, 199401:1–199401:2
https://doi.org/10.1007/s11432-025-4795-1

Nitrogen-vacancy-driven degradation mechanism in ferroelectric wurtzite AlScN

Ruiqing WANG[1], Jiuren ZHOU[1,2*], Xihui YUAN[1,2*], Feng ZHU[3], Siying ZHENG[1,2], Wenxin SUN[1], Xinghui WANG[1], Haiwen XU[1,2], Bochang LI[1,2], Yan LIU[1,2] & Genquan HAN[1,2]

[1]*Faculty of Integrated Circuit, Xidian University, Xi'an 710071, China*
[2]*Hangzhou Institute of Technology, Xidian University, Hangzhou 311200, China*
[3]*TRACE EM Unit and Department of Materials Science and Engineering, City University of Hong Kong, Hong Kong 999077, China*

Received 28 September 2025/Revised 12 December 2025/Accepted 6 February 2026/Published online 13 August 2026

Citation Wang R Q, Zhou J R, Yuan X H, et al. Nitrogen-vacancy-driven degradation mechanism in ferroelectric wurtzite AlScN. Sci China Inf Sci, 2026, 69(9): 199401, https://doi.org/10.1007/s11432-025-4795-1

Ferroelectric wurtzite AlScN, owing to its intrinsic physical advantages, most notably the three-dimensional quasi-single-crystalline lattice and full CMOS compatibility, has emerged as a promising platform for next-generation high-density memory systems [1]. Nevertheless, its practical deployment remains constrained by persistent reliability concerns, including hard breakdown, polarization degradation, and endurance failure, which are theoretically attributed to nitrogen vacancies (V_{N}), rather than metallic vacancies. Despite their central role, direct experimental evidence clarifying the impact of V_{N} is still scarce [2], representing a fundamental bottleneck to the scalable application of wurtzite ferroelectrics.

In this work, we provide direct experimental evidence for the pivotal role of V_{N} concentration in governing the structural and electrical reliability of ferroelectric AlScN. By integrating electron energy-loss spectroscopy (EELS), X-ray diffraction (XRD), and electrical measurements, we reveal that V_{N} accumulation induces lattice distortion, modulates the polarization-switching barrier, and severely limits endurance. These findings clarify the mechanism of V_{N}-driven reliability degradation and establish defect engineering as a key pathway for enabling robust and scalable wurtzite ferroelectric device technologies.

Experiments. To elucidate the critical role of V_{N}, AlScN thin films with different V_{N} concentrations were deposited by reactive magnetron sputtering. The films were grown under a fixed total gas flow of Ar and N_2, while the Ar:N_2 flow fraction was systematically adjusted to 96:96, 64:128, 32:160, and 0:192 sccm, corresponding to samples S1–S4 (Figure 1(a), Appendix A). All other deposition parameters were kept constant to isolate the effect of V_{N} modulation, with vacuum transfer preventing oxygen exposure.

Results and discussion. Figure 1(b) shows the high-resolution transmission electron microscopy (HRTEM) images of S1, grown under the lowest N-plasma condition and therefore expected to contain the highest V_{N} concentration. Notably, even under this condition, the film retains high crystalline quality throughout its thickness, thereby indicating that abundant V_{N} do not compromise the overall structural integrity. To further track vacancy evolution, EELS measurements were carried out on samples S1–S4 across the full film thickness (Figure 1(c), Appendix B). The relative V_{N} concentration was semi-quantitatively estimated by normalizing the nitrogen K-edge intensity (403.1 eV) to the scandium L-edge (407.5 eV), a stoichiometrically stable internal reference. With increasing N-plasma flow, the normalized N-K edge intensity rises progressively from 0.793 (S1) to 0.837 (S4). Energy dispersive X-ray spectroscopy (EDS) also confirms effective modulation of the V_{N} concentration by the nitrogen flow ratio and N-plasma density [3] (Appendix C).

The structural response to this V_{N} modulation was further examined by XRD. As shown in Figure 1(d), the (002) diffraction peak of the wurtzite phase gradually shifts from 36.037° to 35.958° with increasing N-plasma flow, corresponding to an elongation of the *c*-axis lattice constant [4]. In contrast, the in-plane (110) reflection shows negligible variation, demonstrating that strain relaxation is anisotropic and confined mainly along the *c*-axis (Appendix D). This anisotropic lattice response alters the c/a ratio and reshapes the lattice geometry [5]. Corroborating these observations, the combined EELS-XRD analysis in Figure 1(e) underscores the regulatory role of V_{N} in controlling the c/a ratio.

Building on this structural response, particularly c/a ratio modulation, we next examined its impact on polarization switching behavior. Positive-up-negative-down (PUND) measurements were performed on all four samples with nearly identical remanent polarization (P_{r}). As shown in Figure 1(f), coercive field (E_{c}) increases progressively with higher N-plasma density, revealing the influence of V_{N} concentration on the energy barrier for polarization reversal. This trend was further supported by ΔP-E loops and their first derivatives ($\mathrm{d}P/\mathrm{d}E$), which consistently show a shift of the switching peak toward higher fields as nitrogen flow increases (Appendix E). Although the rising E_{c} suggests a trade-off in switching efficiency, this drawback must be considered alongside dielectric breakdown. To provide a more comprehensive reliability

* Corresponding author (email: zhoujiuren@xidian.edu.cn, yuanxihui@xidian.edu.cn)

© Science China Press 2026

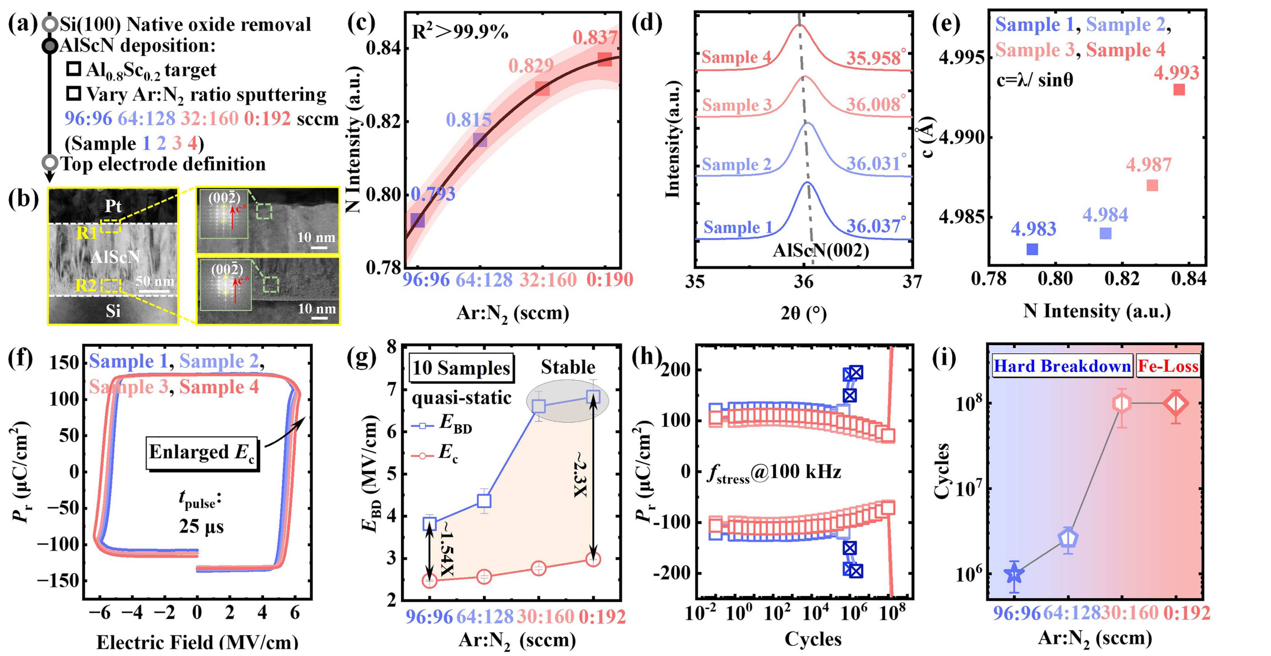

Figure 1 (Color online) (a) Key process flow for AlScN capacitor fabrication. (b) HRTEM images of S1 show high crystalline quality at both the top and bottom interface. (c) EELS spectra for V_{N} concentration analysis in all samples. (d) Effect of Ar:N_2 ratio on (002) peak of XRD patterns. (e) V_{N}-dependent variation of c-axis length. (f) PUND measurements of AlScN samples deposited under different Ar:N_2 gas flow conditions, performed using triangular waveforms. (g) Cumulative quasi-static analyses of E_{BD}, E_{c} and $E_{\mathrm{BD}}/E_{\mathrm{c}}$. (h) Endurance characteristics of varied N_2 flow ratios. (i) Cumulative analyses of endurance, showing a distinct transition with V_{N} concentration.

metric, we introduce the ratio between the breakdown field (E_{BD}) and E_{c} as a figure of merit. Statistical data from quasi-static I-V and C-V measurements across more than ten devices per condition were analyzed. The results show that the $E_{\mathrm{BD}}/E_{\mathrm{c}}$ ratio increases significantly from 154% to 230% as the Ar:N_2 ratio is tuned from 96:96 to 0:192 sccm (Figure 1(g), Appendix F), consistent with the mechanism illustrated in Appendix G. These results validate the systematic improvement in both the switching barrier and dielectric robustness under nitrogen-rich growth conditions.

While such instantaneous metrics offer valuable insight into intrinsic robustness, they do not fully capture long-term reliability, which is critical for ferroelectric memory applications. To address the impact of V_{N} reduction on device reliability, endurance tests were conducted at 100 kHz on all four samples with distinct switching peaks and comparable P_{r} values to ensure consistency. As shown in Figure 1(h), AlScN films grown under nitrogen-deficient conditions suffer premature failure after only $\sim 2\times 10^6$ cycles, whereas those fabricated under nitrogen-rich conditions markedly improve endurance, sustaining up to 1×10^8 cycles. More importantly, nitrogen-deficient samples predominantly undergo abrupt dielectric hard breakdown, whereas nitrogen-rich samples display gradual ferroelectric degradation. This behavioral shift underscores the pivotal role of V_{N} concentration in governing both hard breakdown and fatigue behavior, likely through mechanisms involving vertical V_{N} migration along grain boundaries and ferroelectric domain-wall pinning. Collectively, these findings establish V_{N} concentration as a critical intrinsic factor dictating both the endurance limits and failure pathways of wurtzite ferroelectric devices, directly linking endurance performance (Figure 1(h)) to the V_{N}-regulated failure mechanisms illustrated in Figure 1(i).

Conclusion. By performing the first quantitative analysis of V_{N} in wurtzite AlScN through combined by integrated spectroscopic, structural, and electrical analyses, this study establishes a direct causal link between intrinsic point defects, lattice distortion, and device-level reliability. Our results highlight V_{N} modulation as a fundamental and effective strategy for tailoring the defect-structure-property relationship in wurtzite AlScN ferroelectrics. These insights not only advance the mechanistic understanding of endurance degradation in wurtzite ferroelectrics, but also provide a broadly applicable pathway toward reliable and scalable nitride-based ferroelectric technologies for next-generation memory applications.

Acknowledgements This work was supported in part by National Science and Technology Major Project (Grant No. 2022Z00119002), National Natural Science Foundation of China (Grant Nos. 92264101, 92464205, 62025402, 62090033, 62504178), Major Program of Zhejiang Natural Science Foundation (Grant No. LD25F040004), Postdoctoral Fellowship Program of China Postdoctoral Science Foundation (Grant No. GZC20241309), and Fundamental and Interdisciplinary Disciplines Breakthrough Plan of the Ministry of Education of China (Grant No. JYB2025XDXM105).

Supporting information Appendixes A–G. The supporting information is available online at info.scichina.com and link.springer.com. The supporting materials are published as submitted, without typesetting or editing. The responsibility for scientific accuracy and content remains entirely with the authors.

References

1 Yu X, Zhong N, Cheng Y, et al. Ferroelectric materials, devices, and chips technologies for advanced computing and memory applications: development and challenges. Sci China Inf Sci, 2025, 68: 160401

2 Wang R, Souilamas M, Esfandiar A, et al. In-plane dielectric constant and conductivity of confined water. Nature, 2025, 646: 606–610

3 Zan H W, Yen K H, Liu P K, et al. Effects of Ar/N_2 flow ratio on sputtered-AlN film and its application to low-voltage organic thin-film transistors. Jpn J Appl Phys, 2006, 45: L1093

4 Mayrhofer P M, Eisenmenger-Sittner C, Stöger-Pollach M, et al. The impact of argon admixture on the c-axis oriented growth of direct current magnetron sputtered $Sc_xAl_{1-x}N$ thin films. J Appl Phys, 2014, 115: 193505

5 Ryoo S K, Kim K D, Park H W, et al. Investigation of optimum deposition conditions of radio frequency reactive magnetron sputtering of $Al_{0.7}Sc_{0.3}N$ film with thickness down to 20 nm. Adv Elect Mater, 2022, 8: 2200726